Real Time Textile Fabric Flaw inspection system using Grouped Sparse Dictionary

Xiaohu Wang
Jiangnan University
Benchao Yan
Jiangnan University
Ruru Pan
Jiangnan University
Jian Zhou (jzhou@jiangnan.edu.cn)
Jiangnan University

Research Article

Keywords: Fabric flaw, Sparse representation, Real time inspection, Grouped sparse dictionary

Posted Date: September 27th, 2022

DOI: https://doi.org/10.21203/rs.3.rs-2092464/v1

Real Time Textile Fabric Flaw inspection system using Grouped Sparse Dictionary

Authors: Xiaohu Wang, Benchao Yan, Ruru Pan, Jian Zhou*.

Xiaohu Wang, E-mail: 1030106844@qq.com

Corresponding author: Jian Zhou, E-mail: jzhou@jiangnan.edu.cn

Affiliations: School of Textile Science and Engineering, Jiangnan University. Wuxi 214122, China

Foundation: The National Natural Science Foundation of China [61501209]

Abstract

Fabric surface flaw inspection is essential for textile quality control, and it is demanding to replace human inspectors with the automatic machine vision-based flaw inspection system. To alleviate the time-consuming problem of sparse coding in detecting phase, this work presents a real time fabric flaw inspection method by using grouped sparse dictionary. Firstly, the over-complete sparse dictionary is learned from normal fabric images; Secondly, the learned sparse dictionary is grouped into several sub-dictionaries by evaluating reconstruction error. Finally, the grouped dictionary is used to represent image and identify flaw regions as they cannot be represented well, leading to large reconstruction error. In addition, a non-maximum suppression algorithm is also proposed to reduce false inspection further. Experiments on various fabric flaws and real-time implementation on the proposed vision-based hardware system are conducted to evaluate the performance of proposed method. In comparison with other dictionary learning methods, the experimental results demonstrate that the proposed method can reduce the running time significantly and achieve a decent performance, which is capable of meeting the real-time inspection requirement without compromising inspection accuracy.

Keywords – Fabric flaw Sparse representation Real time inspection Grouped sparse dictionary

1. Introduction

Textile fabric flaws or flaws are generally caused by raw materials (warp or weft yarns), mechanical failures and human factors in the production process. The occurred fabric flaws would seriously impair the quality of final products, leading to a reduction in the sale prices. Thus, the fabric flaw inspection plays a key role in quality control process. At present, the flaw inspection is mainly conducted by human inspectors, suffering from low efficiency and high laboring cost. Therefore, it is of great significance to apply fast and reliable image processing and machine vision techniques to perform automated flaw inspection instead of human.

According to different types of solutions, textile fabric flaw inspection can be mainly divided into five categories [1]: structural methods, statistical method, frequency-domain method, model method, and machine learning method. The structural method obtains structural features by extracting the basic texture structure of the image from the fabric. The existence of defects destroys the original structural texture, and the flaws can be detected by comparing the similarity with the normal texture [2]. Statistics-based methods mainly use the grayscale properties of pixels and their neighborhoods to calculate the statistics in different orders. Commonly used statistical methods are histogram statistics [3, 4], gray co-occurrence matrix [5, 6], mathematical morphology [7] and so on. The spectrum-based method utilizes the similarity between the periodicity of the fabric texture and the spectral characteristics, and applies the method of analyzing the spectrum to the image texture. Fourier transform [8], Gabor transform [9], wavelet transform [10] and so on are commonly used methods. The model-based method is based on the assumption that the texture obeys a specific distribution model and the parameters of the model, so as to judge the image under test according to the specific distribution model, and realize the defect detection, which is suitable for the situation that the surface characteristics of the fabric change irregularly. Common ones are autoregressive models and Markov random fields. The learning-based approach is more adaptable to different fabrics and flaws, which can be further divided into traditional machine learning and deep learning [11]. Traditional machine learning includes support vector machines, dictionary learning [12, 13], etc. On the contrary, deep learning-based methods manage to learn the optimized deep hierarchical features from low to high level for image representation, and

typical models are convolutional neural networks (CNNs), generative adversarial networks (GANs), etc. Although such hierarchy of features learned from deep learning models is quite feasible and powerful, it is time consuming to train those models and a large amount of labelled data is required [14].

Referring to related works, Mak [15] proposes a morphological filter-based defect detection scheme. It uses Gabor wavelet networks to extract features from defect-free images and then matches the optimal morphological filter applied to the same texture background to improve the detection accuracy for different fabric types and defects. Arnia [16] proposed a framework for real-time textile defect detection based on energy and contrast features of the grayscale co-occurrence matrix (GLCM). The proposed framework use DCTb-I to calculate the energy and contrast generated by a small number of DCT coefficients to distinguish if it is a defective patch, and conveniently, there is no need to define thresholds for new textile rolls with different backgrounds. Feng [17] proposed a hardware accelerated algorithm based on a small-scale over-completed dictionary (SSOCD) via sparse coding (SC) method, which is realized on a parallel hardware platform. They use feature segmentation to accelerate SSOCD extraction and improve parallel processing efficiency by optimizing synchronization and communication methods and DSP programs to achieve significant improvements in final detection speed. Wei [18] improved the loss function for image similarity comparison based on VAE in image generation and combined SSIM and L2 to enhance the overall similarity between the generated and input images based on Gaussian patches. And a factory-operated fabric defect detection machine was deployed with excellent practical application. Jia [19] proposed a fabric defect detection system based on migration learning and an improved Faster R-CNN. The improved Faster R-CNN has greatly enhanced detection accuracy and convergence ability, achieving good results for small defects.

Sparse representation theory is widely used in face recognition [20], image denoising [21], target tracking and other fields because of its excellent data feature representation ability. Ma [22] established the target observation model with BOMP as the core, introduced the sparse display into the particle filtering framework, and found the optimal solution after optimization. And the experiments show that this algorithm can still maintain high tracking accuracy and strong robustness in the case that the target appearance changes due to light changes, partial occlusion and pose changes. Kang [23] proposes a generalized adaptive defect detection scheme that uses a random dictionary approach to accommodate fabrics with various textures. This algorithm achieves an average success rate of 100% for the detection of dark-red fabric and dot-patterned fabric.

Sparse dictionary learning method has excellent adaptability to fabrics with different textures and flaws. However, the learning and solving of sparse dictionary take a lot of time, making it difficult to meet the real-time requirements in industrial scenarios. Therefore, this work proposes a dictionary grouping strategy to optimize the sparse dictionary and speed up the sparse coding in inspection stage while guaranteeing the inspection accuracy.

This work is organized as follows: in Section 2, the hardware system of the fabric flaw inspection system is introduced, including the general construction, the light source system, and the image acquisition system. In Section 3, the flow of the flaw inspection algorithm and the strategy of sparse dictionary grouping optimization are described. In Section 4, the experiments on various samples are performed to assess the effectivity of the proposed method. In the last Section, the real-time experiments are conducted to further evaluate the performance of the proposed system.

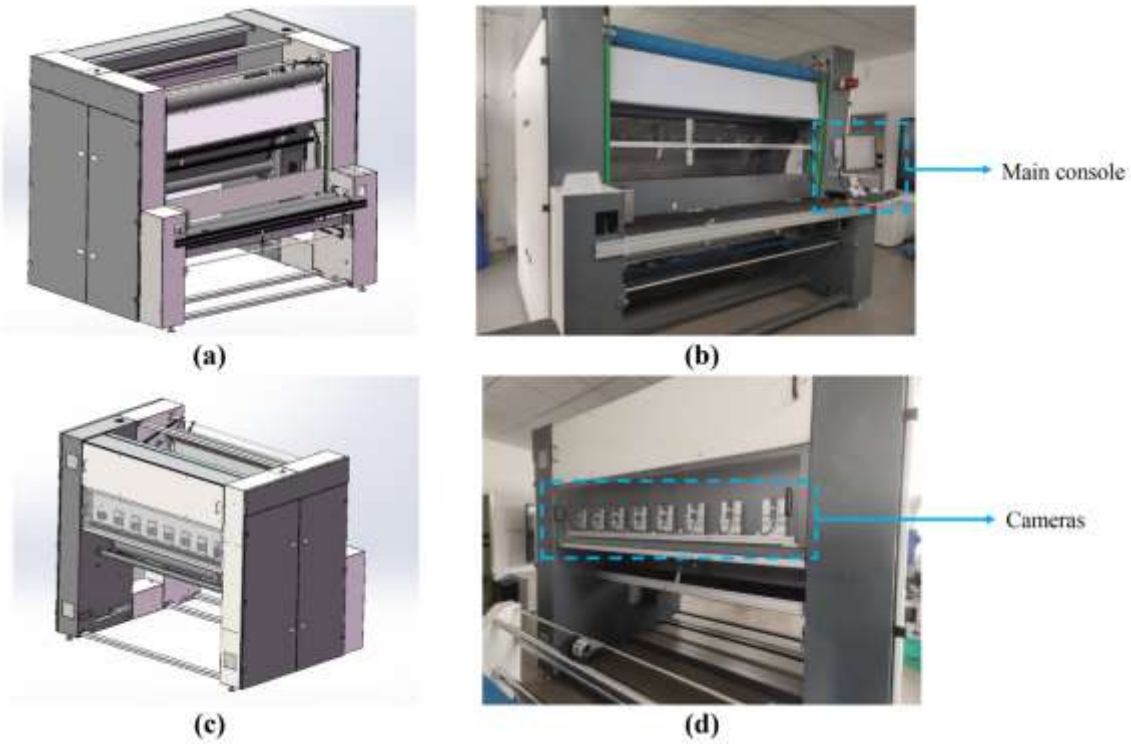

Fig.1 Overview of hardware system: (a) diagram of equipment (front view); (b) front view of equipment; (c) diagram of equipment (rear view); (d) rear view of equipment;

2. Hardware system

2.1 Overview of equipment

As shown in Fig. 1, the schematic diagrams of the equipment are illustrated in Fig. 1(a)(c), whose actual pictures are presented in Fig. 1(b)(d). In the front view, it is mainly designed for operators including main control console, warning lights and fabric driving rollers. In the rear view, there are eight industrial cameras arranged alone a line with a specified interval, in order to cover the full width of a fabric.

2.2 Light source

For a vision-based inspection system, the quality of the images acquired from the cameras in hardware system is highly dependent on the lighting condition, as an appropriateness of illumination is capable of enhancing the features of the flaw areas as prominent as possible.

In order to acquire high quality fabric images for different types of textile fabrics, here the LED light sources supporting external trigger are configured to provide different illumination conditions. From Fig. 2, it can be seen that the fabric can be illuminated under reflected, transmitted and scattered light by switching the light sources. For example, transmitted light is more suitable to capture images with lightweight fabrics, while reflected light is generally for heavyweight ones, such as denim.

2.3 Image acquisition

The camera is a key device of the vision-based inspection system of fabric flaw inspection, and the quality of the acquired images directly affects the later identification and extraction of flaw information.

Compared with the line scan camera cannot generate a complete image at once, the image accuracy may be affected by the impact of scanning motion accuracy, thus affecting the measurement accuracy of the disadvantages. The area scan camera captures the two-dimensional matrix information at once, and eliminates the feedback link between scanning motion and position of the line camera, making the measurement more direct, accurate and efficient. In this work, the image acquisition system deploys eight area cameras (MER-502-79U3M, having 502 Megapixels and 79 fps) in order to capture the full width of the textile fabric, whose mounting diagram is illustrated in Fig. 3.

From Fig. 3, it can be seen that the eight cameras are mounted along a line with a minor view overlap (about 18mm), which is able to capture maximum fabric width up to 2.2m with

resolution of 8.4pixel/mm (213PPI). To minimize its dimension, the mirrors are utilized to change the direction of the incident light to cameras (see Fig. 2(a)).

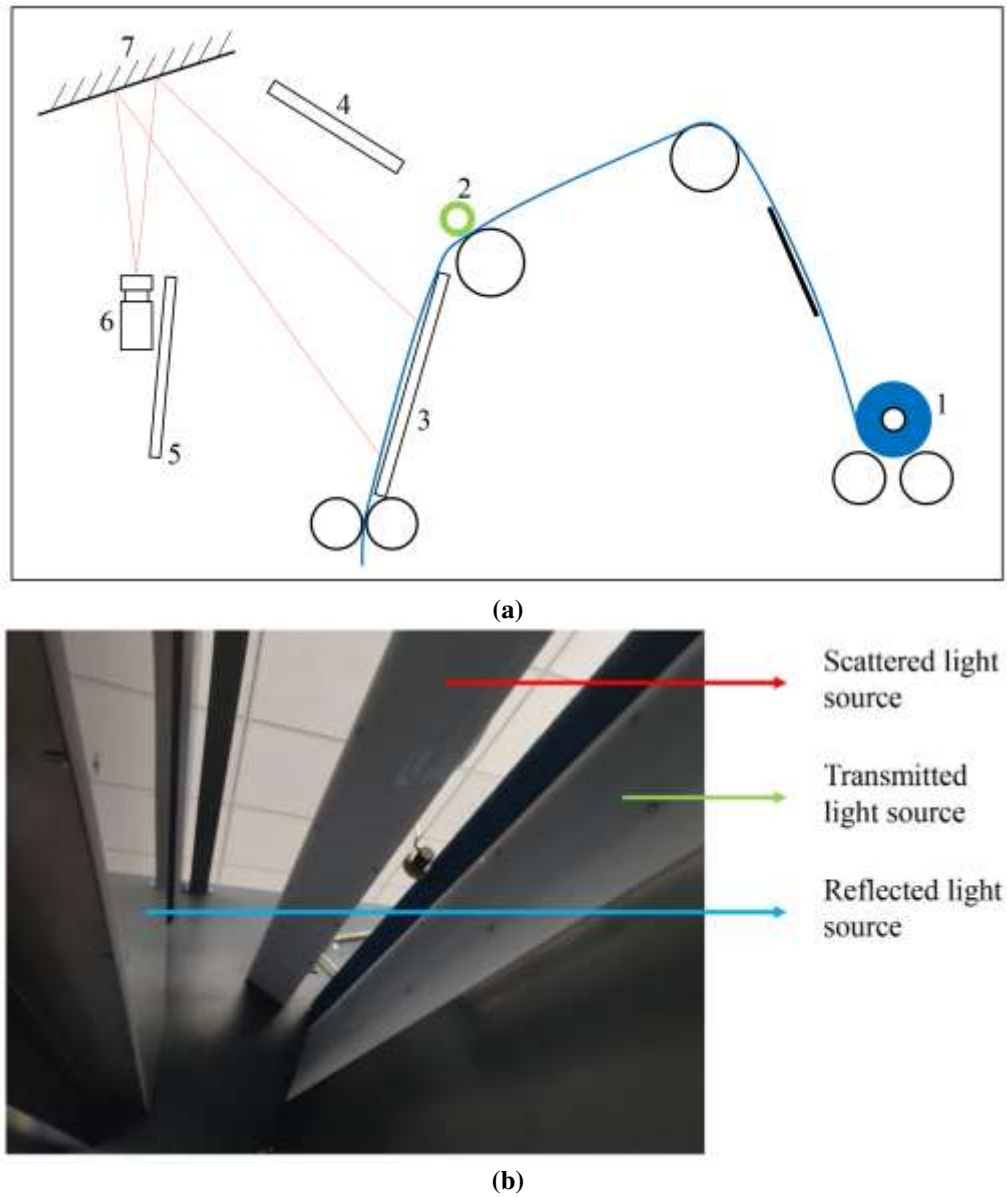

(a)

(b)

Fig.2 Light sources system

(a) Diagram of LED light source:1-Fabric; 2-Encoder; 3-Transmitted light source; 4-Scattered light source; 5-Reflected light source; 6-Camera; 7-Mirror.

(b) Actual picture

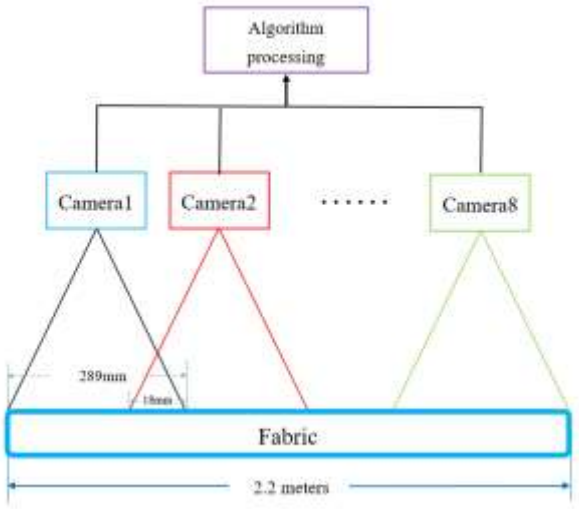

Fig.3 Diagram of the acquisition system

3. Methodology

3.1 Sparse representation theory

In the field of signal processing, signals can usually be decomposed into linear combinations of some basis elements or functions for representation. The basic idea of linear representation of a fabric texture signal is to find some basis elements (i.e., dictionary atoms) whose linear combinations can be optimally approximated (reconstructed) for the original signal under certain constraints. The resulting sparse dictionary can be better adapted to the signal features by learning, allowing dictionary learning to represent the input signal more efficiently. For textile defect inspection, such a representation can more effectively restore the fabric features or structure, highlighting the defective parts and facilitating the subsequent identification of defective areas.

The sparse representation usually uses an overcomplete dictionary, which the number of dictionary elements is larger than their feature dimension, and the sparsity of the feature expression is only a small number of elements in the overcomplete dictionary. Assuming that the overcomplete dictionary size is K, it can be expressed as $D=[d_1,d_2,\ldots,d_k]\in \mathrm{R}^{n\times K}$, in which each column $d_k \in R^n$ is an atom, and the data matrix is X. Let α be the coded sparse matrix, and write as $\alpha=[\alpha_1,\alpha_2,\ldots,\alpha_n]\in \mathrm{R}^{K\times n}$, at this time, $X\approx D\times\alpha$, if there are only $T(T=K)$ non-zero numbers in α_i. The solution of the sparse dictionary can be viewed as a mathematical optimization problem with some approximation condition as the objective function, and usually the l_0 is relaxed to l_1 for the solution, and the sparse coding problem under D is known as Formula (1).

$$\min_{\alpha\in_{\mathrm{i}}^{K\times n}} \frac{1}{2}\| X-D\alpha \|_F^2 +\lambda \| \alpha \|_1, \quad (1)$$

where λ is the regularization parameter that controls the weight of the reconstruction error $\|X-D\alpha\|_F^2$ with respect to the sparsity degree $\|\alpha\|_1$. When the dictionary D is determined, the LARS algorithm can be used to solve the sparse coefficients.

3.2 Overview of the proposed method

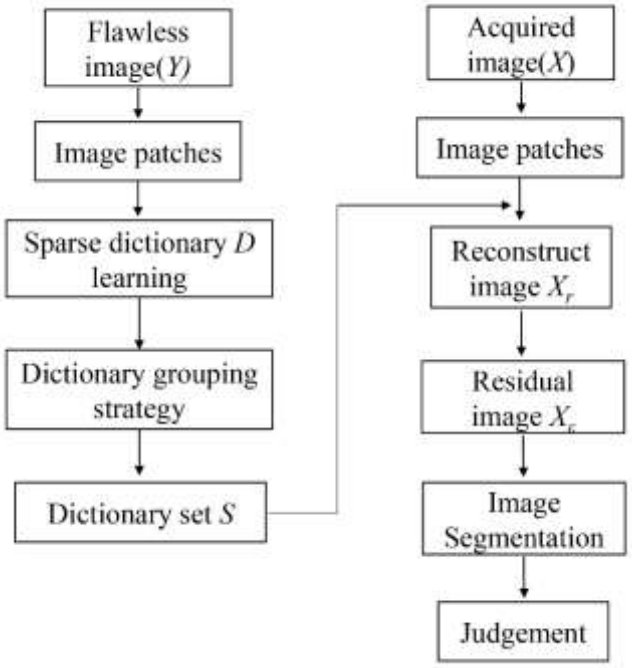

Fig. 4 Algorithm flow chart

As seen in Fig. 4, the proposed algorithm can be divided into two stages. In the learning stage, the input is the flawless fabric images Y and divided into image patches of a certain size, which are combined into a data matrix after unfolding into column vectors. Sparse dictionary learning is performed on the data matrix, then we obtain sparse dictionary D and select dictionary elements from D to combine into sub-dictionaries by dictionary grouping strategy (see the next section for details) as a dictionary set $S=\{S_1, S_2, ..., S_q\}, S_i\in \mathrm{R}^{n\times t}$ for subsequent use, which t is the number of dictionary elements.

In the test stage, the acquired image X is also divided into image patches and combined into a matrix. The corresponding coefficient is solved by using the least square method from S_i. The reconstructed image X_r can be obtained by Formula (2).

The residual image X_ε containing potential flaw regions can be obtained by subtraction operation, which is given by Formula (3).

$$X_{ri} = D \times \alpha_i \tag{2}$$

$$X_\varepsilon = \| X_t - X_{ri} \|^2 \tag{3}$$

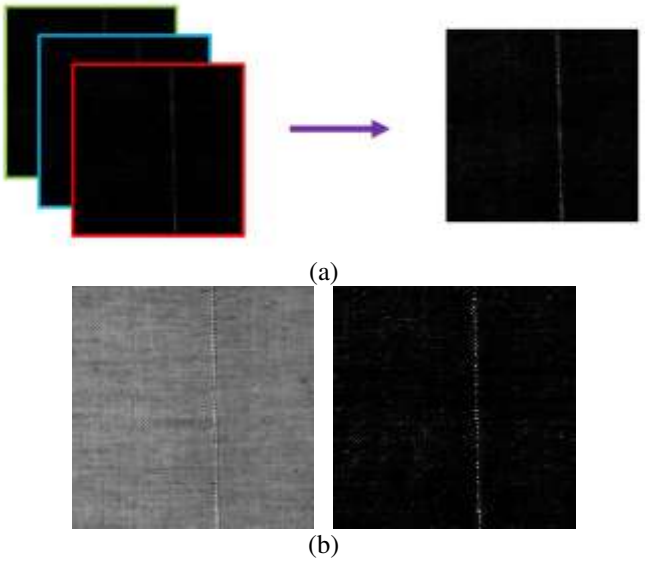

Fig. 5 An example of residual image
(a) Fusion of residual images; (b) Defective image and its residual image

As there are q groups in set S, the total of q residual images will be obtained, and they are fused into a single image X_ε by adding operation, which is shown in Fig. 5(a). For the residual image in Fig. 5(b), the patch strategy is used to locate defective regions, which will be discussed in the next section.

3.3 Parameter selection

As the defective regions are located in patch-level, it is necessary to find a proper size of the image patch. If the patch is too small, it cannot contain the complete fabric texture information, but the abnormal features of flaws can be well highlighted; if the patch is too large, the proportion of the defective area in the patch is limited, though it is beneficial for representing the fabric texture. Here, the patch size of 16×16 pixels and 32×32 pixels are tested to demonstrate their effects in inspection performance, whose results are shown in Fig. 6.

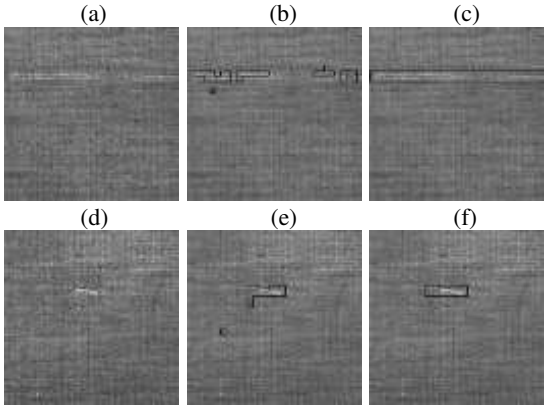

Fig. 6 Inspection results under different patch sizes.(a) warp flaw; (b)(c)Inspection result of (a) using patch sizes of 16×16 pixels and32×32 pixels); (d)weft flaw;(e)(f) Inspection result of (d) using patch sizes of 16×16 pixels and 32×32 pixels); (g) Blocky flaw; (h)(i) Inspection result of (g) using patch size of 16×16 pixels and 32×32 pixels

From the above results, it is clear that the patch of 32×32 pixels can achieve better performance than that of 16×16 pixels for different kinds of flaws. For the patch size with 16×16 pixels, the defective areas will be broken into several patches, thus losing the differentiable defective textures, resulting in poorer inspection results. Considering the imaging resolution (8.4 pixel/mm), the patch with 32×32 pixels is equal to the physical dimension about 3.8mm×3.8mm, which is suitable for identifying those flaws like commonly occurred linear defects with width about 1mm (quarter of patch size).

Moreover, the size of the sparse dictionary K needs to be determined as well, and the reconstruction error is used as the index. Fig. 7 shows the results for different K (128, 256, 512, 1024, 1248).

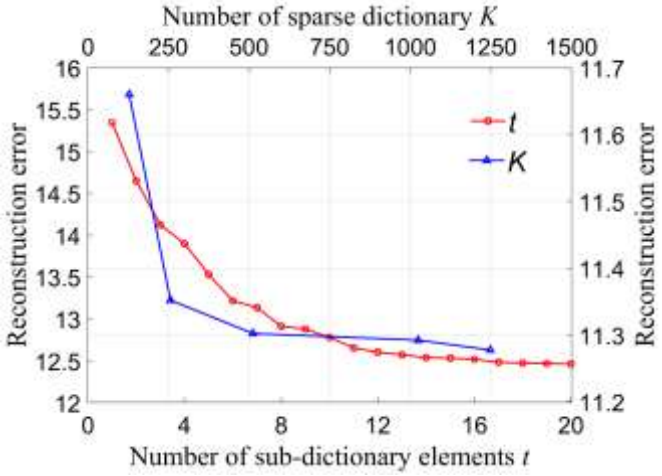

Fig. 7 Reconstruction error with different K and t: K corresponds to the right y-axis; t corresponds to the left y-axis

From Fig. 7, the curve of K versus reconstruction error corresponds to the right y-axis, and the curve of t versus reconstruction error corresponds to the left y-axis. it can be seen that the reconstruction errors are significantly reduced when K

is large than 200, becoming stable after K>512 thus the sparse dictionary size is set to K=512.

Similarly, the reconstruction error is also used to find the proper number dictionary elements t in each dictionary groups. Theoretically, the increase of t is good for restoring the fabric texture and reducing the reconstruction error. But on the other hand, if t is too large, it is likely to introduce the defective region into the dictionary elements, which makes the defective regions being approximated well.

For different fabric types, the number t of combined dictionaries t is needed to change to achieve the best reconstruction effect. From Fig. 7, for the fabrics used in this work, the reconstruction error no longer decreases rapidly after t >8, becoming stable after it. Thus, in order to ensure the inspection effect and speed, t=14 is selected under comprehensive consideration.

3.4 Dictionary grouping strategy

Having obtained the dictionary parameters K and t, the dictionary grouping strategy is presented in Algorithm 1.

The proposed algorithm proceeds through iterations, where each iteration selects a sub-dictionary whose the size has been chosen previously. In each iteration, the dictionary element combination in a sub-dictionary attempt to represent as many training data as possible, and in this way the dominant sub-dictionary combination of the most common features can be found more quickly. And the remaining data that cannot be well represented by this sub-dictionary will go to the next cycle and be represented by other combinations. At the end of this process, all the training data are well represented, and the criterion for evaluating a good representation is controlled by the reconstruction error bound L.

In Algorithm 1, the input includes the image patches X from normal images, learned sparse dictionary D, the number of sub-dictionaries elements t, the reconstruction error bound L. First initialize the number of iterations and select dictionary elements from the learned sparse dictionary to combine into a sub-dictionary S_1, and determine whether sub-dictionary S_1 meets our requirements by Formula (4). Generally speaking, S_1 not only meets the requirements but also represents most of the image patches X. Then, the reconstruction error of the image patches below the bound is removed, X gets updated and goes to the next iteration. Then keep repeating the previous steps, each iteration picks a sub-dictionary S_i and determines whether S_i is available by Formula (4). In the end, all the image patches are removed until X becomes an empty set, the output is a dictionary set $S=\left\{S_1,\ S_2,\ ...,\ S_q\right\}, S_i \in \mathrm{R}^{n\times t}$.

In particular, the number of iterations represents the number of sub-dictionaries in the dictionary set S, and the general number is around 5. Here, the upper limit of the number of iterations is set to 8, because too many sub-dictionaries will affect the inspection speed. Considering that S_i may fail to represent any image patches, the solution is to replace the image and adjust the number of sub-dictionary elements t.

$$S_i=\begin{cases} S_i & \left\|X-S_i\alpha\right\|_F^2 \le L \\ \varnothing & \text{otherwise} \end{cases} \tag{4}$$

Algorithm 1 Dictionary grouping algorithm

Input: Image patches $\boldsymbol{X}$ from normal images, learned sparse dictionary $\boldsymbol{D}$, number of sub-dictionaries elements t, reconstruction error bound L.

Output: Grouped dictionary set $\boldsymbol{S}$=$\{S_1, S_2, ..., S_q\}$

Initial i=1
repeat
  repeat
    Randomly select t dictionary elements from $\boldsymbol{D}$ as S_i
    Update S_i according to Formula (4)
  until $S_i \neq \varnothing$
  Add S_i to dictionary set $\boldsymbol{S}$
  Update $\boldsymbol{X}$ if the patches that satisfy $\left\|X-S_i\alpha\right\|_F^2 \le L$ are removed from $\boldsymbol{X}$
  i=i+1
until $X=\varnothing$

As described in Algorithm 1, the first sub-dictionary S_1 are able to approximate most of the patches, and all patches are gradually approximated in each iteration. There are overlapping parts in the elements of different sub-dictionary combinations in the dictionary set S, and most sub-dictionaries can represent the most common features of the fabric, but for some image

patches, one sub-dictionary cannot represent and another sub-dictionary can reconstruct well, so the sub-dictionaries can achieve a complementary effect between them and can reconstruct the image excellently.

3.5 False inspection suppression

Since the defective image cannot be reconstructed well by the learned dictionary, such areas will presents a larger reconstruction error than others in the residual image. Therefore, for the residual image X_ε, the defective patches can be segmented by assuming that its background pixels can be modeled by a Gaussian distribution. Then, the threshold *Th* can be determined by the following Formula.

$$Th=\mu+c\times\tau \tag{5}$$

where μ and τ are mean value and standard deviation of image patches of residual image X_ε, c is a predefined constant.

Normally, in detecting stage, any patch whose pixel value larger than *Th* will be treated as flaws. Owing to undesired noise, when using low threshold value, it is prone to treat normal patch as flaws, resulting in high false inspection rate. To address this limitation, an algorithm to suppress the false inspection is designed with reference to the principle of non-maximum suppression.

In the non-maximum suppression, the target inspection frames have their corresponding scores, and eventually a frame with the highest score is selected [23]. Here the segmented defect patch is viewed as the target inspection frame, and the corresponding reconstruction error is the score, whose suppression algorithm is listed in Algorithm 2.

In Algorithm 2, The input includes the defective patches B_t after segmentation and corresponding reconstruction error C_t, control coefficient σ. Firstly, it is to find the maximum reconstruction error and its corresponding patch in current image, which is the most likely to be true defect. Then multiply the reconstruction error with the set control factor to get a threshold value δ. Then, all defective patches are divided into two categories according to δ. The first category belongs to defective patches with reconstruction errors c_i larger than the threshold δ, and taken them as true flaws, while the second category containing patches are all detected falsely, needing to be removed. In addition, there is also a case that all the flaws are in the first category, which means that the reconstruction errors of the defective patches do not have significant difference, and it is justified to think that all of them are false inspections. Because the real flaw is generally greatly different from the fabric structure, and the reconstruction error should be very large and prominent, and some examples are presented in Fig. 8

Algorithm 2 Suppression of false inspection

Input: Defective patches and reconstruction error after threshold segmentation. $B_t=[b_1,b_2,\ldots,b_n]$, $C_t=[c_1,c_2,\ldots,c_n]$.Control coefficient σ.

Output: $B_t=[b_1,b_2,\ldots,b_m]$.

1: Compute threshold $\delta=\sigma\times\max[b_1,b_2,\ldots,b_n]$
2: **For** $i=1\rightarrow n$ **do**
3: **if** $c_i>\delta$ **then**
4: Remove b_i in B_t
5: **end if**
6: **end for**
7: **if** $m=n$ **then**
8: $B_t=\varnothing$
9: **return** normal
10: **end if**
11: **return** $B_t=[b_1,b_2,\ldots,b_m]$

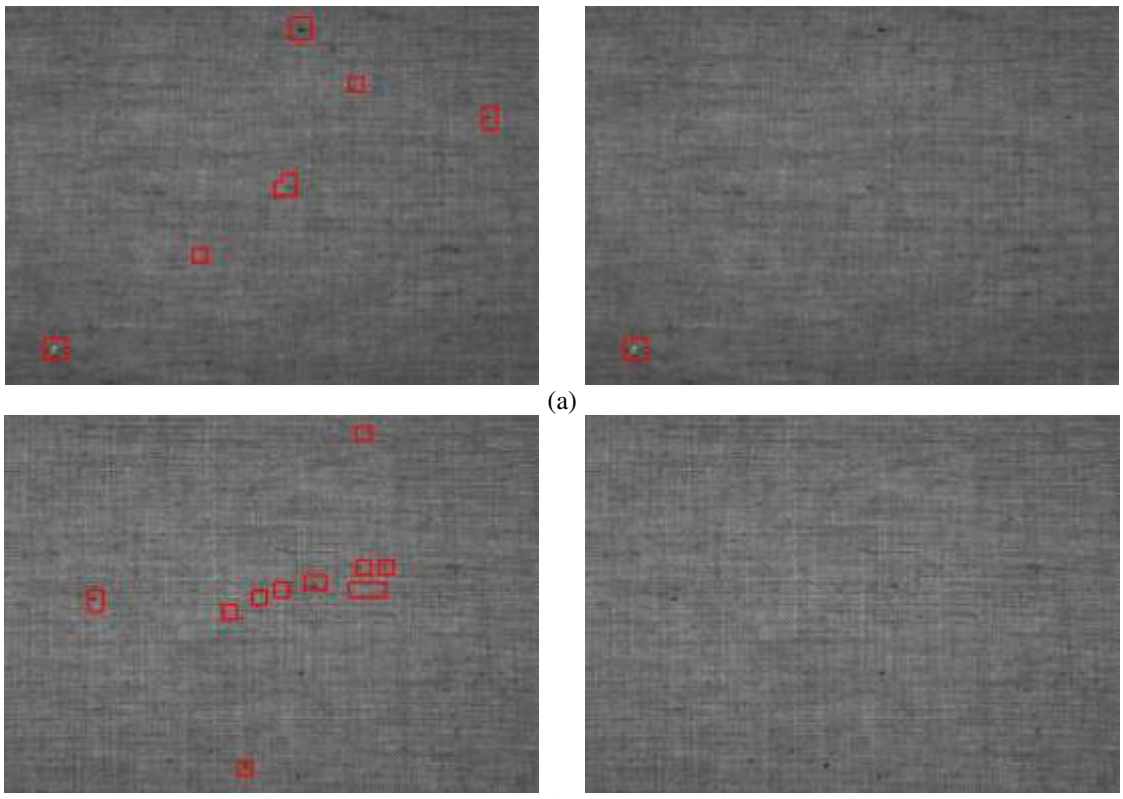

Fig. 8 Example of false inspection suppression
(a) Image with flaws;(b) Images without flaws

As seen in Fig. 8(a), the reconstruction error of the patches containing flaw is much different from that of patch without flaws, so it is easy to discriminate them from normal patches, suppressing the true flawless patches being mistakenly treated as flaws. In Fig. 8 (b), it is a normal image actually, and the reconstruction errors of patches are close to each other, and they are prone to be mistakenly treated as defective patches without using Algorithm 2. It is suggested that, the proposed algorithm can perform well in suppressing false inspection.

4. Experiment

4.1 Dataset

To validate the performance of the proposed method in offline case, all fabric images are captured by the aforementioned fabric inspection equipment (see Fig. 1), with the fabric rolls coming from production line. The total length of a fabric roll is about 160m and the width of 1.6m. All eight cameras' acquisition resolution are set to 2432×896 pixels, which corresponds to an actual size of 28.9cm×10.7cm. For continuous image capture of each camera, the actual overlapping height of two adjacent frames is about 10mm. Thus, there are total of 4628 captured fabric images, including 621 images with flaws. In order to evaluate the performance of the proposed method objectively, images with similar appearance of flaws are removed, and a total of 230 defective images are selected for testing, including warp flaws, weft flaws and blocky flaws. And a total of 700 flawless images selected from normal images are used for evaluating false inspection rate, which is about three times number of the defective images. Fig. 9 shows the typical captured flawless and flaw images with a size of 512 × 512 pixels.

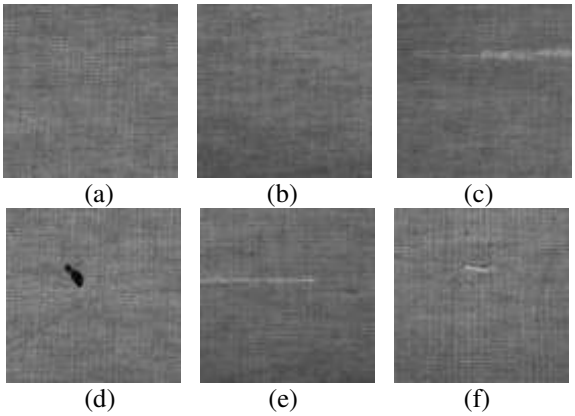

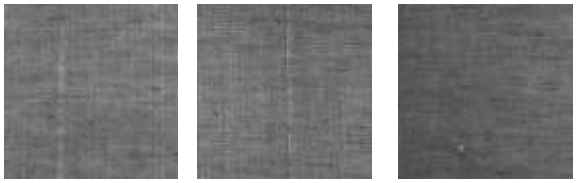

(g) (h) (i)

Fig. 9 Flawless and typical defective images
(a)(b) Flawless. (c)(e) Weft flaws. (d)(f)(i) Block flaws. (g)(h) Warp flaws.

All the 230 images used in the experiment are cropped into a size of 512 × 512 pixels, and divided into four categories: 120 images of warp flaws, 53 images of weft flaws, 57 images of block flaws and 700 flawless images. Here, the inspection performance of the proposed method is evaluated at the patch level, i.e., the images of dataset are cut into image patches, and each of them is viewed as a sample, and the effects of the patch size has been discussed above, and half overlap means that the image is segmented into 32 × 32 pixels patches with half of the patch width and height overlapping (16 pixels), e.g., a 512 × 512 pixels image can be segmented into 961 patches.

In experiment, two related dictionary-based methods are performed for comparison, which are the unconstrained dictionary (UD) method and the sparse dictionary (SD) method. The UD is that does not impose any constraints on the dictionary elements, while the SD method adds an l_1 regularization term to the dictionary learning. The proposed method uses the grouped dictionary (GD) as described in the previous section. All three methods have used the false inspection suppression algorithm proposed.

Sparse dictionary solution has to choose a suitable regularization parameter λ to control the weight of reconstruction error $\|X - D\alpha\|_F^2$ with the sparsity degree $\|\alpha\|_1$. Empirically, the experiments demonstrate that the sparse dictionary can achieve a good reconstruction effect for most images at λ = 0.6, and the number of dictionary elements used to reconstruct patches is around 12.

In summary, the parameters involved in all methods are chosen as follows: the number of UD elements is 14; the number of SD elements is 512, and the regularization parameter λ=0.6; the GD method contain 5 dictionaries with 14 elements inside. All experiments are implemented in Matlab (2018a) with Intel Core i5-6300HQ and 8G RAM.

To objectively evaluate the performance of the proposed method in detecting flaws, two evaluation metrics are used, the correct inspection rate (CDR) and the false inspection rate (FDR).

$$\mathrm{CDR} = \frac{N_p}{N_{df}} \times 100\% \tag{6}$$

$$\mathrm{FDR} = \frac{N_e}{N_{nf}} \times 100\% \tag{7}$$

where N_p is the number of defective samples detected correctly and N_{df} is the total number of defective samples; N_e is the number of normal samples false detected as defective samples and N_{nf} is the total number of normal samples.

4.2 Result and discussion

A comparison of the inspection results of the three methods is listed in Table 1, and visualized examples of inspection results are shown in Fig. 10. Three methods have used the false inspection suppression algorithm are used for the other two method as well.

Table 1 Summary of fabric flaw inspection results

Method	Overlap mode	Warp flaw		Weft flaw		Block flaw		Normal	Average		Time(ms)
		CDR(%)	FDR(%)	CDR(%)	FDR(%)	CDR(%)	FDR(%)	FDR(%)	CDR(%)	FDR(%)	
UD	half overlap	90.00	0.67	90.57	0.89	89.29	0.69	0.84	89.57	0.81	54.6
	no overlap	90.83	0.66	90.57	0.81	91.07	0.61	0.81	90.43	0.79	14.4
SD	half overlap	99.17	0.11	96.23	0.21	94.64	0.16	0.35	96.96	0.33	41268.2
	no overlap	98.33	0.09	96.23	0.21	94.64	0.14	0.34	96.52	0.33	10413.9
GD	half overlap	97.50	0.18	94.34	0.35	96.43	0.21	0.43	96.09	0.41	125.1
	no overlap	96.67	0.16	92.45	0.32	96.43	0.18	0.42	95.22	0.39	32.2

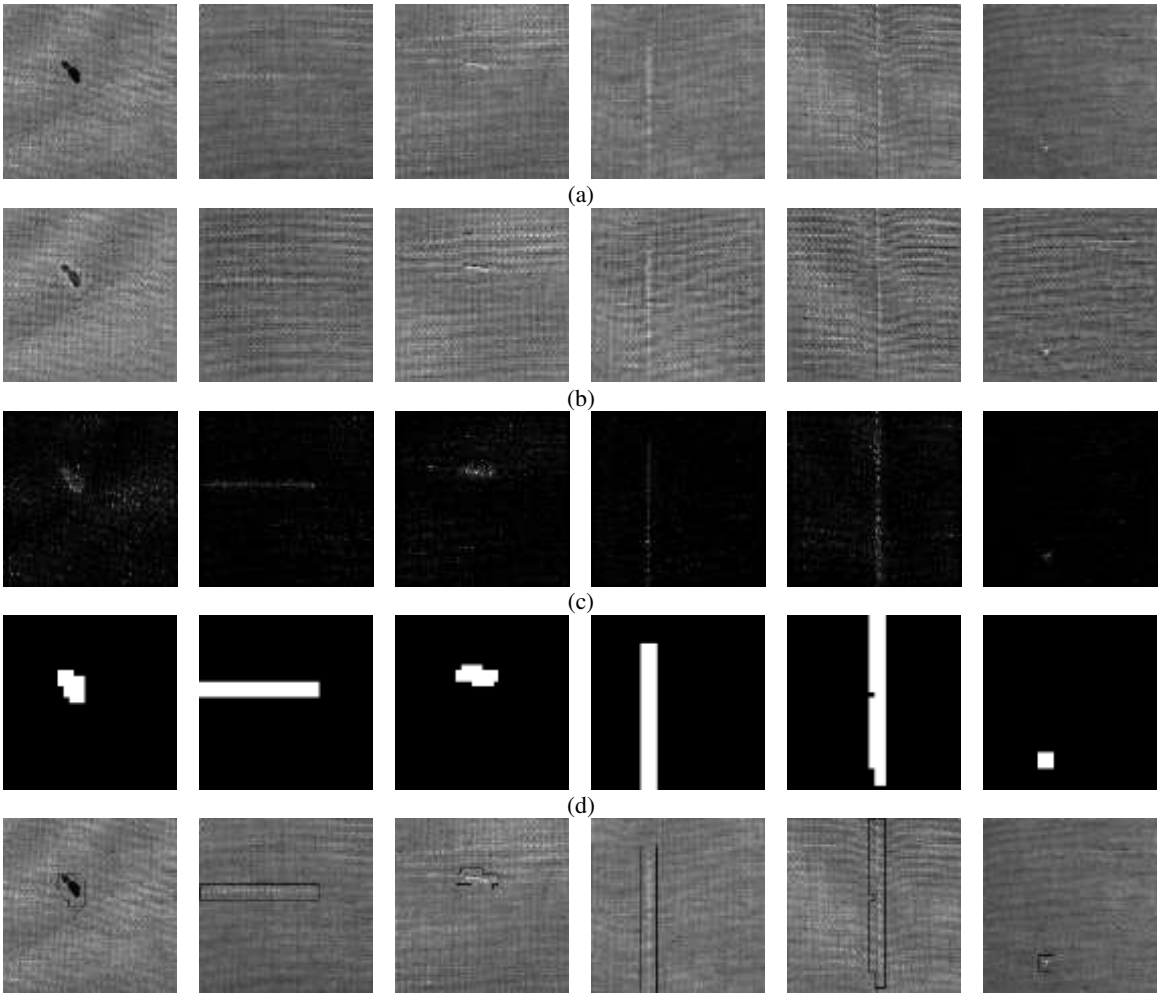

Fig. 10 Examples of inspection results. (a)Input images. (b)Reconstructed images. (c)Residual maps. (d)Binary images. (e)Inspection results

As listed in Table 1, it can be seen that three methods have high CDR for different types of flaws, and the best results are obtained for warp flaws. The FDR of the dataset is close to the FDR of the normal dataset, the reason is that this static experiment takes patches as samples, and the size of the defective parts of the images containing flaws in the dataset is different, and the remaining normal patches after removing the defective patches are much smaller than the samples of the normal set. The table shows that the SD method takes an average of 41268.2ms for one image, which is the most time-consuming among them, while the UD method takes an average of 54.6ms, taking shortest processing time. Compared to UD method, the proposed method spends more time in computing residual images in grouping dictionary, but its running time is extremely faster than that of SD method. Theoretically speaking, the proposed method and UD method can both meet the requirements of real-time inspection, but the CDR of the UD is lower than GD method, while the SD method achieve the highest CDR. The possible for it may be that the SD do not use all dictionary elements patches each time, but selecting the least number of elements for patch approximation, helping ignoring details such as defective areas. Similarly, the possible reason why GD also achieves a competitive CDR is that the proposed dictionary grouping strategy is equivalent to the process of selecting the optimal dictionary elements for sparse dictionary in advance, and each dictionary combination is able to be complementary to each other. The FDR and the CDR contradict with each other, the higher the CDR achieves, the lower the FDR would be, thus under the same CDR, the proposed method is slightly higher FDR than the SD method, while computing time is almost 300 times faster than it.

As shown in Fig. 10, it can be seen that the parts of defective regions are inevitably recovered in the reconstructed versions of detective images (see in Fig 10(b)) due the powerful representation of the learned grouped dictionary, but it is sufficient to discriminate the defective areas from background in patch-level(see in Fig. 10(c)). It also indicates that the grouped dictionary is not only capable of representing normal fabric textures, but maintain the discriminative power for defective patches.

In summary, in terms of inspection accuracy, the proposed method is in the middle of the sparse dictionary method and the unconstrained dictionary method, but it can achieve an acceptable inspection accuracy with the lowest computation burden, rendering it capable of being used those real-time industrial inspection applications.

5. Deployment

To evaluate the dynamic performance of the proposed algorithm and hardware system, the proposed algorithm is deployed on the inspection system, and the aforementioned fabric roll with length of 160m and width of 1.6m is used for experiment. In order to ensure the full coverage of entire fabric, the two adjacent image frames share an overlap of about 10mm in image height direction as same as section 4.1. As external trigger mode is used to trigger image acquisition, the camera's acquisition frame rate and LED light source frequency are automatically adjusted based on the speed encoder moving with the fabric synchronously. The image resolution is set to 2432×896, which corresponds to an actual size of 28.9cm × 10.7cm. At this resolution, it takes about 104ms to process one frame without parallel computation and the non-overlapping patch. Theoretically, the machine can run at a maximum speed up to 62m/min. To ensure accuracy and stability, the deployed algorithm runs at a speed of 20m/min for online inspection experiment.

As full width of fabric is captured, it is necessary to remove the fabric selvages. Here, the background subtraction is used to crop the fabric selvages automated. With the aid of background image, the selvages can be located by find the peaks of the mean gray level value of image along column. Fig. 11 illustrates an example of finding location of the selvages.

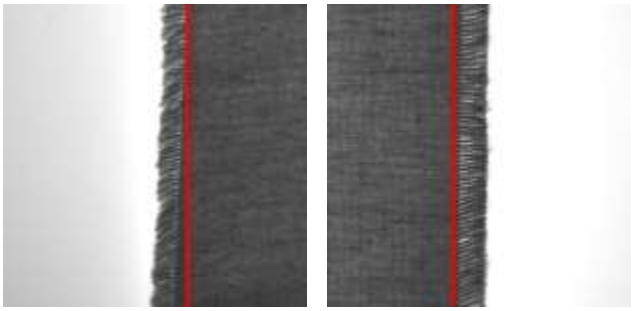

(a) (b)

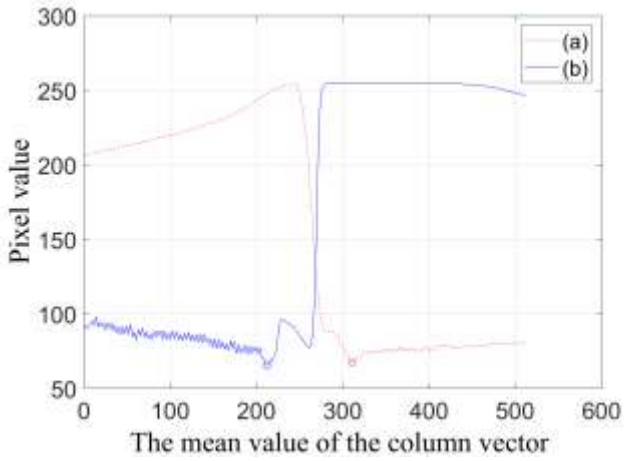

(c)

Fig. 11 Fabric selvage removal

The algorithm is coded in C++ by Microsoft Visual Studio (2015), and implemented on Intel(R) Core(TM) i9-9900K CPU @ 3.60GHz, 16G RAM.

The evaluation metrics CDR and FDR are still used, but computed in image-level. Since the SD method is too time-consuming and can't meet the real-time flaw inspection, this experiment only tests the performance of UD and GD, and the real time test results are listed in the Table 2.

Table 2 Summary of real-time inspection results

Method	Overlap mode	Suppress false inspection	CDR (%)	FDR (%)	Time (ms)
UD	half overlap	yes	90.18	1.50	39.5
		no	90.02	2.28	38.3
	no overlap	yes	88.57	1.35	10.6
		no	88.89	1.85	10.1
GD	half overlap	yes	96.30	0.93	413.1
		no	96.30	1.15	411.3
	no overlap	yes	94.85	0.85	104.2
		no	95.17	1.03	102.4

From Table 2 it can be seen that the use of overlap scheme is able to improve CDR compared to that of nonoverlap mode, meanwhile increasing processing time and reducing the FDR slightly but can be ignored. The use of the false inspection suppression algorithm can significantly reduce FDR, especially for non-overlap mode. Compared with the previous static experiment, the CDR of this real-time inspection experiment is slightly improved, while the FDR is significantly increased.

The reason for this is that the FDR are calculated in image-level, different from the previous static experiment where the patch level is used. Since the majority of flaw regions some of For flaw images, it can be correctly detected only if the majority of flaw regions are truly classified as a flaw the defective parts in an image are detected, the image can be regarded as correctly detected, making the slight improvement of CDR. Similarly, Since the regions of flaws generally occupies a small percentage of whole fabric image, the increase of normal images will reduce FDR eventually, and evaluation performance based on image-level is equivalent to the reduction in the amount of normal samples.

Fig. 12 shows the proposed flaw inspection machine, and Fig. 13 shows the results of the flaw inspection using GD in real time case. From the results in Fig. 13, it can see that there are some false inspections, which are mistakenly treated as the flaws, due to the effects of cotton knots in the pure cotton fabric, which can be removed after washing.

6. Conclusions

With the growing demand for surface flaw inspection on industrial products, a vision-based hardware system and the grouped sparse dictionary method have been proposed to address the real time flaw inspection problem on textile fabric. By converting the time-consuming sparse coding into a least square problem, the proposed method has been proved to be capable of reducing computation time in inspection phase significantly. In order to further reduce false inspection rate, a non-maximum suppression algorithm was also presented. The results on offline experiments shown that the method proposed can increase the detecting speed hundreds of times compared to spare dictionary, and achieve a decent performance compared to other two related methods. For the real-time implementation, experiments on 160m fabric demonstrated that the proposed method is able to meet the real time inspection requirement, and achieve a comparable performance with respect to that of offline case.

Fig.12 The deployed machine.

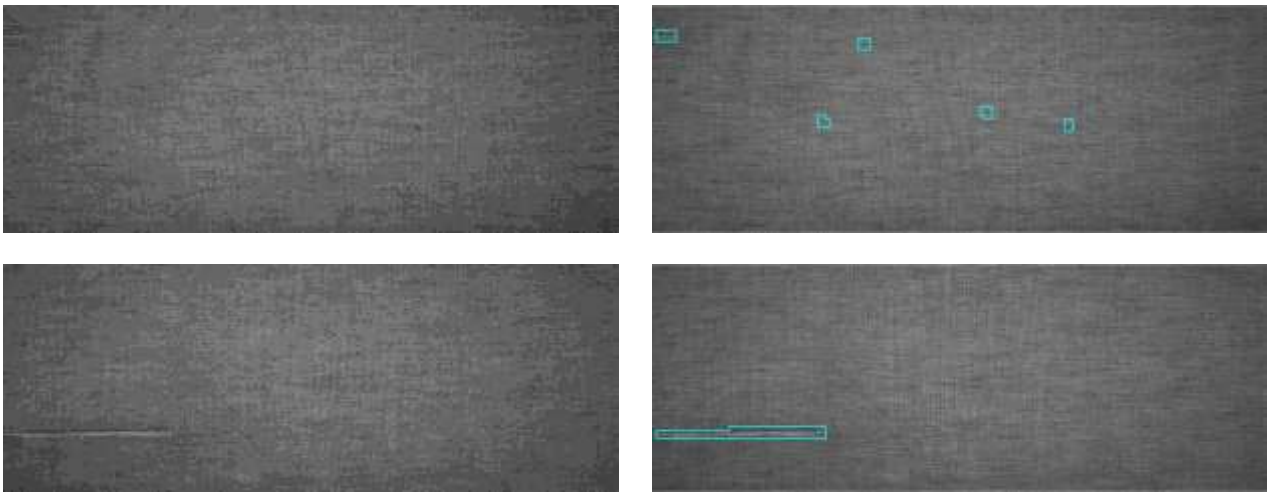

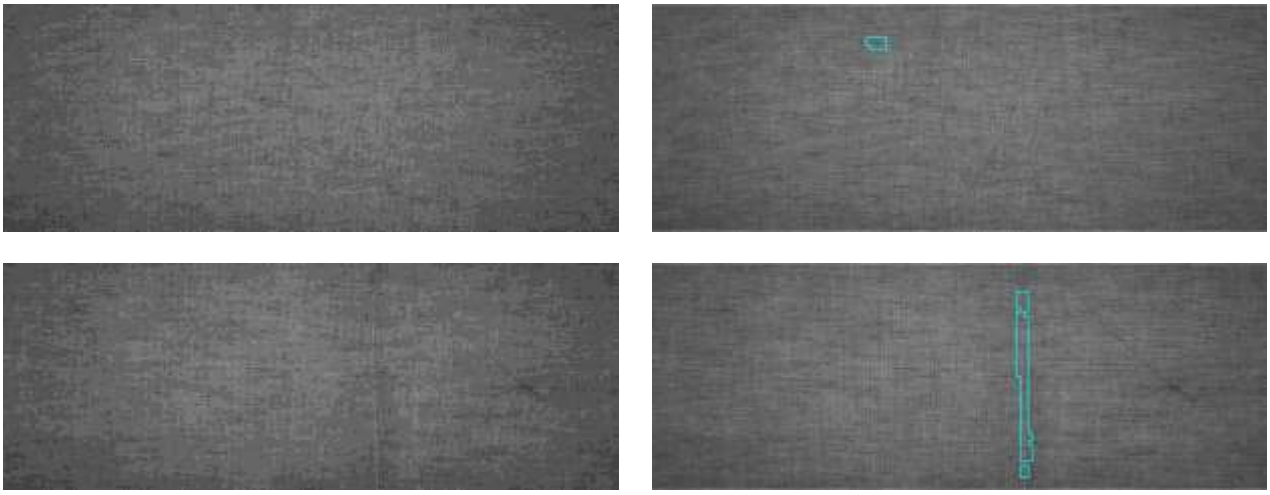

(a) (b)

Fig.13 Detect example in the deployed machine. (a)Input image. (b)Inspection result.

References

1. Lv, W.T., Lin, Q.Q., Zhong, J.Y., Wang, C.Q., Xu, W.Q.: Research progress of image processing technology for fabric defect detection. Journal of Textile Research. **42**(11), 197-206 (2021). https://doi.org/10.13475/j.fzxb.20200702710
2. Divyadevi, R., Kumar, B.V.: Survey of automated fabric inspection in textile industries. In: 2019 International Conference on Computer Communication and Informatics (ICCCI), pp. 1-4 (2019). https://doi.org/10.1109/ICCCI.2019.8822180
3. Gao, G, Zhang, D., Li, C., et al.: A novel patterned fabric defect detection algorithm based on GHOG and low-rank recovery. In: 2016 IEEE 13th International Conference Signal Process (ICSP). IEEE, pp. 1118-1123 (2016). https://doi.org/10.1109/ICSP.2016.7878002
4. Li, C., Gao, G., Liu, Z., et al.: Defect detection for patterned fabric images based on GHOG and low-rank decomposition. IEEE Access. **7**, 83962-83973 (2019). https://oi.org/10.1109/ACCESS.2019.2925196
5. Zhu, D.D., Pan, R.R., Gao, W.D., et al.: Yarn-dyed fabric defect detection based on autocorrelation function and GLCM. Autex Research Journal. **15**(3), 226-232 (2015). https://doi.org/10.1515/aut-2015-0001
6. Deotale, N.T., Sarode, T.K.: Fabric Defect Detection Adopting Combined GLCM, Gabor Wavelet Features and Random Decision Forest. 3D Res. **10**, 1-13 (2019). https://doi.org/10.1007/s13319-019-0215-1
7. Rebhi, A., Abid, S., Fnaiech, F.: Fabric defect detection using local homogeneity and morphological image processing. In: 2016 International Image Processing, Applications and Systems (IPAS). IEEE, pp. 1-5 (2016). https://doi.org/10.1109/IPAS.2016.7880062.
8. Ren, H.H., Jing, J.F., Zhang, H.H., et al.: Cross-Printing Defect Detection of Printed Fabric Using GIS and FTDT. Laser & Optoelectronics Progress. **56**(13), 94-99 (2019).
9. Li, Y.D., Zhang, C.: Automated vision system for fabric defect inspection using Gabor filters and PCNN. SpringerPlus. **5**(1), 1-12 (2016). https://doi.org/10.1186/s40064-016-2452-6
10. Li, Z.X., Zhou, J., Pan, R.R., et al.: Fabric defect detection using monogenic wavelet analysis. Journal of Textile Research. **37**(9), 59-64 (2016).
11. Şeker, A., Peker, K.A., Yüksek, A.G., Delibaş, E.: Fabric defect detection using deep learning. In: 2016 24th Signal Processing and Communication Application Conference (SIU). IEEE, pp. 1437-1440 (2016). https://doi.org/10.1109/SIU.2016.7496020
12. Wu, Y., Wang, J., Zhou, J.: Sparse representation of woven fabric texture based on discrete cosine transform over-complete dictionary. Journal of Textile Research. **37**(9), 59-64 (2016).
13. Zhou, J., Semenovich, D., Sowmya, A., Wang, J.: Sparse Dictionary Reconstruction for Textile Defect Detection. In: 2012 11th International Conference on Machine Learning and Applications. **1**, 21-26 (2012). https://doi.org/10.1109/ICMLA.2012.13
14. Zhu, Z.W., Han, G.J., Jia, G.Y., et al.: Modified dense Net for automatic fabric defect detection with edge computing for minimizing latency. In: IEEE Internet of Things Journal. **7**(10), 9623-9636 (2020).
15. Mak, K.L., Peng, P., Lau, H.Y.K.: Optimal morphological filter design for fabric defect detection. In: 2005 IEEE International Conference on Industrial Technology, pp. 799-804 (2005). https://doi.org/10.1109/ICIT.2005.1600745
16. Arnia, F., Munadi, K.: Real time textile defect detection using GLCM in DCT-based compressed images. In: 2015 6th International Conference on Modeling, Simulation, and Applied Optimization (ICMSAO). IEEE, pp. 1-6 (2015). https://doi.org/10.1109/ICMSAO.2015.7152203
17. Feng, T., Zou, L., Yan, J., et al.: Real-Time Fabric Defect Detection Using Accelerated Small-Scale Over-Completed Dictionary of Sparse Coding. International Journal of Advanced Robotic Systems. **13**(1), (2016). https://doi.org/10.5772/62058.
18. Wei, W., Deng, D., Zeng, L., et al.: Real-time implementation of fabric defect detection based on variational automatic encoder with structure similarity. J Real-Time Image Proc. **18**, 807–823 (2021). https://doi.org/10.1007/s11554-020-01023-5.
19. Jia, Z., Shi, Z., Quan, Z., et al.: Fabric defect detection based on transfer learning and improved Faster R-CNN. Journal of Engineered Fibers and Fabrics. **17**, (2022). https://doi.org/10.1177/15589250221086647
20. Fanaee, F., Yazdi, M. & Faghihi, M.: Face image super-resolution via sparse representation and wavelet transform. SIViP. **13**, 79–86 (2019). https://doi.org/10.1007/s11760-018-1330-9
21. Lu, T., Li, S., Fang L., et al.: Spectral–Spatial Adaptive Sparse Representation for Hyperspectral Image Denoising. IEEE Transactions on Geoscience & Remote Sensing. **54**(1), 373-385 (2016). https://doi.org/10.1109/TGRS.2015.2457614.
22. Ma, W., Xu, F.: Study on computer vision target tracking algorithm based on sparse representation. J Real-Time Image Proc. **18**, 407–418 (2021). https://doi.org/10.1007/s11554-020-00999-4.
23. Kang, X., Zhang, E.: A Universal and Adaptive Fabric Defect Detection Algorithm Based on Sparse Dictionary Learning. IEEE Access. **8**, 221808-221830 (2020). https://doi.org/10.1109/ACCESS.2020.3041849.
24. Yang, Y., Song, H., Sun, S., et al.: A fast and effective video vehicle detection method leveraging feature fusion and proposal temporal link. J Real-Time Image Proc. **18**, 1261–1274 (2021). https://doi.org/10.1007/s11554-021-01121-y